JOURNAL OF MATERIALS SCIENCE 35 (2000) 6105–6110

Melt processing of superconducting $YBa_2Cu_3O_{7-\partial}$ thick films on AgPd substrates via atmosphere control

T. C. SHIELDS, J. S. ABELL
School of Metallurgy and Materials, University of Birmingham, Birmingham, B15 2TT, UK
E-mail: T.C.Shields@bham.ac.uk

T. W. BUTTON
IRC in Materials for High Performance Applications, University of Birmingham, Birmingham, B15 2TT, UK

W. HAESSLER, G. RISSE, K. FISCHER, L. SCHULTZ
IFW Dresden Institute of Solid State and Materials Research, D-01171 Dresden, Germany

Superconducting $YBa_2Cu_3O_{7-\partial}$ (123) c-axis textured thick films have been prepared on AgPd substrates by a modified screen printing and melt processing method. Heating the samples in an inert gas (N_2) has enabled melt processing to take place at lower temperatures than conventional YBCO thick film processing in O_2. The atmosphere is switched to $p(O_2) = 100\%$ at peak temperature in order to initiate the crystallisation of the 123 phase. Variation in properties of the films with changes in the peak processing temperature has been investigated. Samples processed at peak temperatures of $\geq$980°C show better microstructures and superconducting properties than those processed at lower temperatures. Quenching experiments have also been performed in order to investigate further the phase relationships and crystallisation mechanism of the 123 phase.
© *2000 Kluwer Academic Publishers*

1. Introduction

Melt processed superconducting thick films of $YBa_2Cu_3O_{7-\partial}$ (YBCO, 123) prepared by the screen printing or doctor blade methods have been extensively studied over the past few years. Their potential applications include those utilising the microwave properties of the films [1, 2], and certain power engineering applications [3]. Most thick film fabrication has involved melt processing in O_2 above the peritectic reaction of YBCO on ceramic substrates such as yttria-stabilised zirconia (YSZ).

Recently biaxially textured thin films of YBCO have been prepared on textured metallic substrates with buffer layers by using RABiTS (rolling assisted biaxially textured substrates) [4, 5] and IBAD (ion beam assisted deposition) [6, 7]. RABiTS involves the production of a textured metallic substrate onto which textured buffer layers and YBCO films are deposited by "thin film" techniques. In IBAD thin films of textured buffer layers are deposited on polycrystalline metallic and ceramic substrates, followed by YBCO.

Both routes employ vacuum-based PVD techniques which are not easily scaleable: thick film coating technology is an attractive commercial alternative if it can produce bi–axially textured layers. Recent work [8] has suggested that thick films of YBCO on {110}⟨110⟩ textured Ag substrates have some degree of biaxial texturing which is thought to be seeded by the Ag substrate. This processing is executed in a low $p(O_2)$ environment in order to partially melt the YBCO at a temperature lower than the melting point of silver [9]. It is known that the peritectic reaction temperature can be lowered by using low $p(O_2)$ [10]. The films are heated above the peritectic temperature into the 211 + L phase field and then slowly cooled down under the same $p(O_2)$ in order to crystallise the 123 phase.

Alternatively, thick films can be heated in low $p(O_2)$ into the partially molten phase field and then the introduction of high $p(O_2)$ will drive the crystallisation of the 123 phase [9, 10], by passing into a region of the phase diagram where the 123 phase is stable. This is the method used in the present study, in which the samples are heated in N_2 and then the gas is switched to O_2 at the peak temperature (T_{peak}). The phase diagram after Krabbes *et al.* [10] is shown in Fig. 1 to illustrate the method. In order successfully to employ metallic substrates in this way it is necessary to understand the phase relationships and formation mechanisms of this type of processing. In this study, we have used polycrystalline AgPd substrates, which have the advantage of having a higher mechanical strength and higher melting point than pure silver [11], thus increasing the processing temperature window. Previous work [12] has shown the importance of the deleterious reaction between AgPd

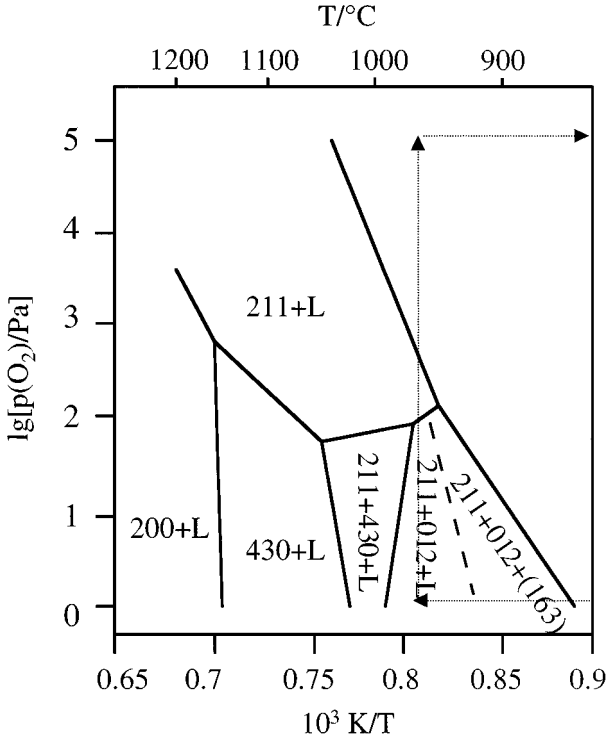

Figure 1 Phase diagram showing stability of 123 as a function of temperature and $p(O_2)$, after Krabbes *et al.* [10]. A typical combination of temperature and $p(O_2)$ experienced during processing is illustrated by the path indicated.

and YBCO in air. Therefore a knowledge of the 123 formation mechanism could result in a reduced time at the lower temperatures involved in low $p(O_2)$ processing, thus reducing the reaction between film and substrate. The aim of the paper is to present the results of processing YBCO thick films on AgPd substrates by heating in N_2, and switching to O_2 at peak temperature.

2. Experimental

YBCO thick films have been prepared by screen printing commercial stoichiometric YBCO powder (Rhone Poulenc Superamic Y123 N13K-30-90) on polycrystalline $Ag_{0.85}Pd_{0.15}$ substrates. The dimensions of the films were 25 mm × 5 mm with a green thickness of approximately 30 μm. The samples were placed in a conventional thick film processing tube furnace on a Pt sample stage. An attached Pt/Rh thermocouple enabled accurate measurement of the sample temperature. A summary of the heat treatment procedures is given in Fig. 2. The organic binder was burnt out at 400°C in flowing O_2 before switching to flowing N_2. Rapid gas switching was ensured by the use of mass flow controllers. The samples were held at 400°C until the $p(O_2)$ reading was less than 100 ppm on the zirconia cell O_2 analyser situated at the output of the furnace. The samples were heated at 5°C/min to T_{peak} in N_2, and held for 5 min in order for the temperature to stabilise. The gas was switched to O_2, and the samples were held at T_{peak} for a further 5 min, the time taken to reach $p(O_2) = 100\%$. The flow rate was 2l/min for both N_2 and O_2 atmospheres. T_{peak} was varied between 950°C and 1000°C at intervals of 10°C, and its influence on the

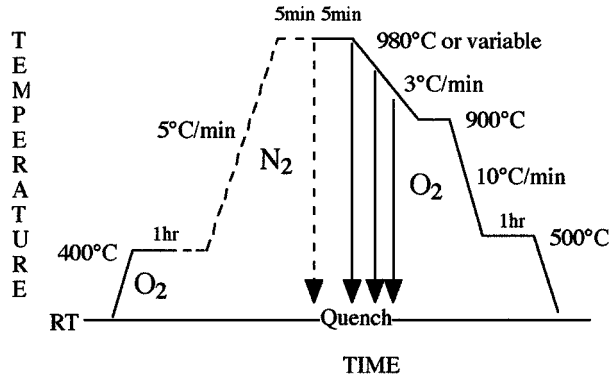

Figure 2 Summary of the heat treatment procedures of the thick films. The dashed lines indicate processing in N_2.

microstructure and properties has been studied. From the peak temperature the samples were cooled down to 900°C at 3°C/min, and subsequently to 500°C at 10°C/min. Samples were finally oxygenated by holding at 500°C for 1hr in O_2. A typical combination of temperature and $p(O_2)$ experienced during this thermal profile is illustrated by the path indicated in Fig. 1. The change in $p(O_2)$ in switching from N_2 to O_2 drives the crystallisation of the 123 phase.

In order to understand more fully the formation mechanism of these films, samples have also been quenched from various temperatures. The system design enabled rapid cooling by pulling the sample straight out of the furnace hot zone to room temperature in the same atmosphere. A wire was attached to the Pt sample stage, and this wire passed through a long silica tube at the output of the furnace. To achieve quenching the sample was pulled along the tube from the hot zone to outside the furnace.

The microstructures of the films have been assessed using X-ray diffraction (XRD) and scanning electron microscopy (SEM) with energy dispersive X-ray analysis (EDX). The transition temperature (T_c) and critical current density (J_c) have been measured using AC susceptibility and four point probe measurements respectively.

3. Results and discussion

3.1. Crystallisation experiments

The XRD investigations have shown that the *c*-axis texture of the films is dependent on the value of T_{peak}. The 00l peaks are enhanced for values of $T_{peak} > 970$°C. Fig. 3 compares 2 films, fired below and above 970°C. Fig. 3a shows an XRD pattern for a film fired below 970°C, namely 960°C, and it is seen to be characteristic of untextured material. Fig. 3b shows a typical XRD pattern of a film fired above 970°C, namely 980°C. The 00l peaks can be seen to be of greater intensity compared to the 013/103 peak, indicating *c*-axis texture. It is also worth noting that $BaCuO_2$ peaks are identified in the XRD patterns.

There are also differences in the surface microstructures of the samples in the two temperature regimes. At values of $T_{peak} < 970$°C the films are characterised by small rectangular grains (Fig. 4a). At these temperatures there is clearly not enough

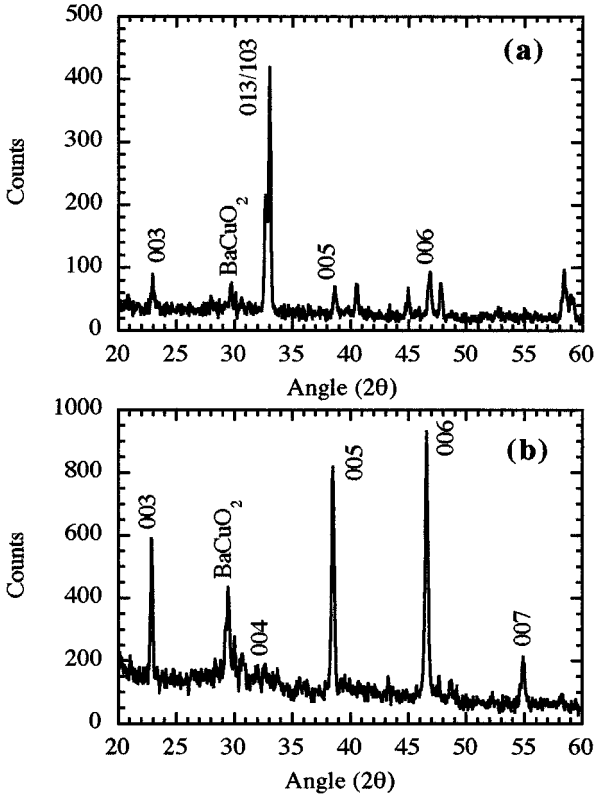

Figure 3 Typical XRD patterns of films fired with peak temperatures (a) <980°C ($T_{peak} = 960$°C) and (b) ≥980°C ($T_{peak} = 990$°C). Peaks have been indexed to the 123 phase and $BaCuO_2$ reflections labelled.

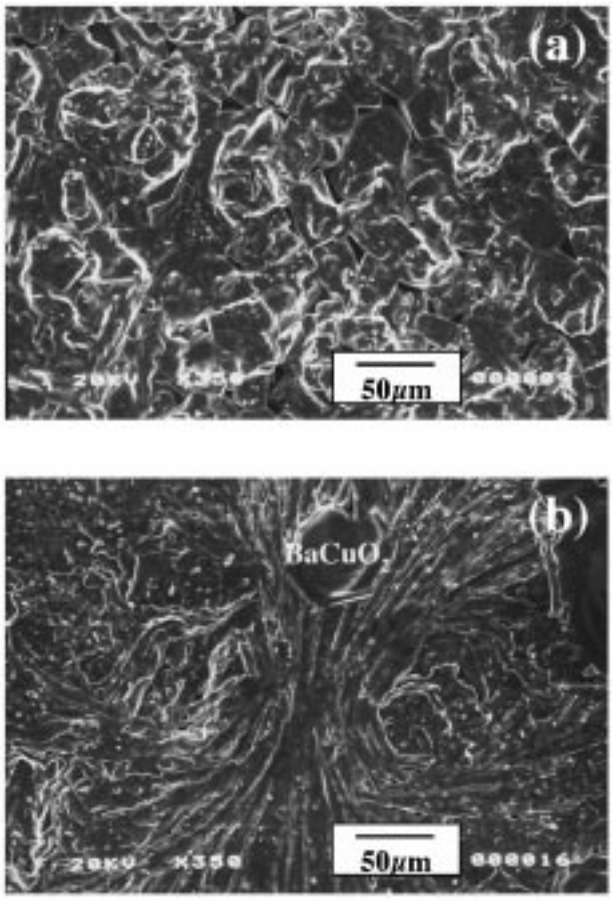

Figure 4 Typical SEM surface microstructures of films fired with peak temperatures (a) <980°C ($T_{peak} = 960$°C) and (b) ≥980°C ($T_{peak} = 1000$°C).

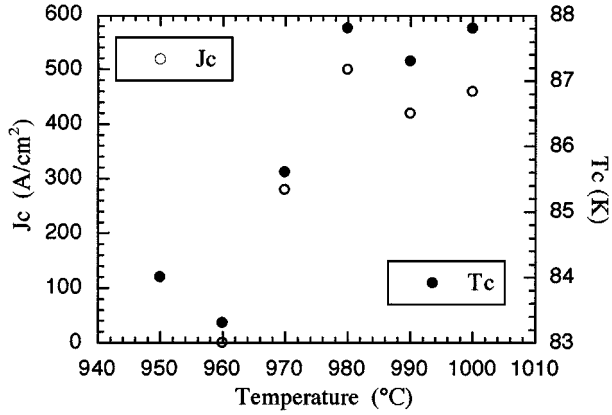

Figure 5 T_c and J_c behaviour as a function of peak temperature.

liquid phase for melt texturing to occur. Above 970°C a wheat sheaf microstructure can be seen (Fig. 4b), typical of YBCO thick films on ceramic substrates [13], where melt processing occurs in O_2 at above 1025°C. This type of microstructure is thought to occur as a result of relatively fast cooling through the peritectic, in combination with large amounts of undercooling [9]. In the present study melt texturing is occurring at a temperature lower than 1025°C because of initial heating in the N_2 atmosphere i.e. low $p(O_2)$ (<100 ppm). Large regions of $BaCuO_2$ identified by EDX analysis can also be observed on the surface of films fired above 970°C. The $BaCuO_2$ originates from the Ba-Cu rich liquid in the 211 + L region of the phase diagram (Fig. 1). These $BaCuO_2$ regions are generally not observed on thick films on YSZ substrates [13], because any $BaCuO_2$ present is thought to react with the substrate forming a $Ba(Zr,Cu)O_3$ reaction layer.

There is a correlation between the microstructures and the electrical properties. The transition temperature T_c and the critical current density J_c of the samples, are plotted against peak firing temperature in Fig. 5. Both T_c and J_c are seen to increase above 970°C. It is unclear why the T_c values are greater for films processed at higher temperatures. However similar behaviour has been observed for YBCO thick films on YSZ substrates, where films fired above the peritectic have higher T_c's than those fired at lower temperatures [14]. It should also be noted that the values of J_c in this study are relatively low compared to undoped YBCO thick films on YSZ substrates [2]. The values are approximately 3 times lower, and may be attributed to Pd contamination from the substrate. This will be discussed in more detail later.

Some films were also heat treated completely in N_2, with no switch to O_2 at T_{peak}, and on cooling were found to be non-superconducting, due to the lack of 123 crystallisation. Although according to Krabbes *et al.* [10] the 123 phase is expected, in practice it appears difficult to achieve these equilibrium conditions. Similar behaviour was found in bulk samples in the previous study [10].

3.2. Quenching experiments

Results are now reported on samples (a) heated in N_2 and quenched from T_{peak} before and after the switch

to O_2, and (b) samples quenched from various temperatures (T_{quench}) below T_{peak} during cooling in O_2. A T_{peak} of 980°C was chosen, as this temperature resulted in films with *c*-axis texture and the highest J_c values (Fig. 5). A summary of the phases found in the quenched samples is given in Table I.

(a) The cross-sectional microstructures of the samples quenched in N_2 and O_2, from T_{peak} are shown in Fig. 6. For the sample quenched in N_2 the phases 211 and $BaCu_2O_2$ (012) have been positively identified from SEM EDX analysis (Fig. 6a). The XRD pattern indicated that only $BaCO_3$ is seen on the surface of the film. It is possible that $BaCO_3$ forms as a result of degradation of the $YBa_6Cu_3O_{10.5}$ (163) phase, which is known to be unstable in moisture and CO_2 [15], or from the degradation of the corresponding liquid. However it should be stressed that the 123 decomposition mechanism is not fully understood. There is no direct evidence for 163 in either this or the previous study [10]. In the previous study the presence of 163 was assumed from phase rule considerations. Its lack of detection was attributed to it's extreme sensitivity with moisture. It is not clear whether quenching from T_{peak} in N_2 occurs in a region where the suggested 163 phase is in the solid phase or has melted (Fig. 1).

It is also worth noting that, at this point in the heat treatment procedure there is no evidence for chemical interaction between the film and substrate, suggesting little liquid phase present at 980°C in N_2.

On switching to O_2 and quenching, the microstructure is dramatically changed (Fig. 6b). No 123 phase is crystallised immediately on switching to O_2; instead 211, $Ba(Cu,Pd)O_2$, CuO and BaCu rich phases have been identified. The presence of these phases in this sample suggests the film has passed through the 211 + L region of the phase diagram. The liquid in this region is known to be Ba and Cu rich. This peritectic reaction is responsible for the melt texturing seen in YBCO thick films on YSZ substrates [2, 13], albeit at higher temperatures. At this stage in the process there is evidence for chemical interaction between the film and substrate. The interaction is a result of the Ba-Cu rich liquid produced on switching to O_2. This interaction is manifested in the $BaCu(Pd)O_2$ phase present on the surface of the films, Cu in the substrate, and Ag–rich particles within the matrix of the film. It should, however, be noted that there is no continuous reaction layer at the film/substrate interface, as is seen in the case of YBCO thick films processed on YSZ substrates [2, 13].

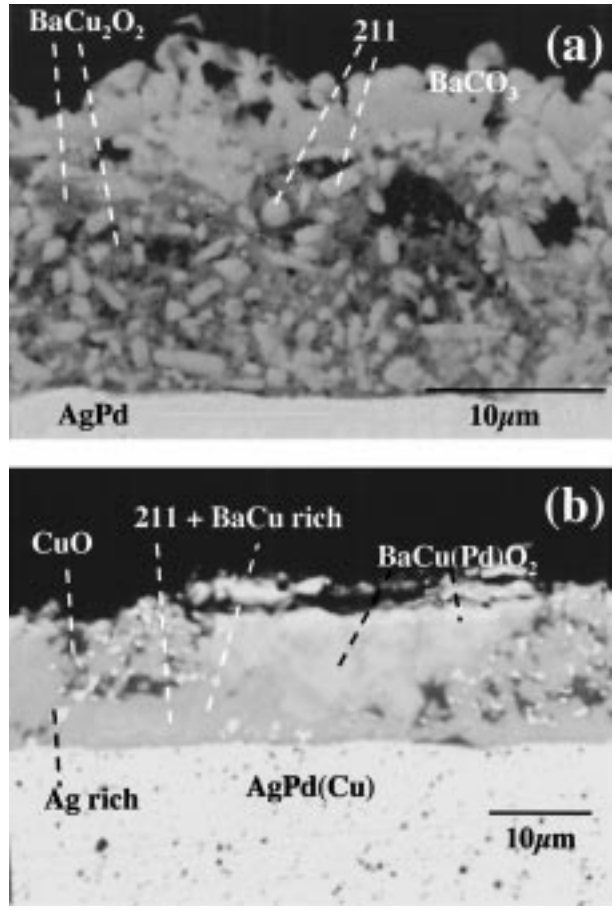

Figure 6 Cross-sectional microstructures of samples quenched from 980°C (a) in N_2; 211, $BaCu_2O_2$ and $BaCO_3$ phases have been identified (b) in O_2; 211, CuO, $BaCu(Pd)O_2$, and BaCu rich phases have been identified, there is also a small amount of Cu present near the surface of the substrate.

TABLE I List of YBCO thick films on $Ag_{0.85}Pd_{0.15}$ substrates and phases identified for samples quenched from different temperatures

T_{quench} (°C)	XRD	SEM
980 N_2	$BaCO_3$	012, 211, AgPd, $BaCO_3$
980 O_2	$BaCuO_2$ + ?	211, BaCu rich, $BaCu(Pd)O_2$, CuO, Ag, AgPd(Cu*)
965 O_2	$BaCuO_2$ + ?	211, BaCu rich, $BaCu(Pd)O_2$, CuO, Ag, AgPd(Cu*)
950 O_2	$BaCuO_2$ + ?	211, BaCu rich, $BaCu(Pd)O_2$, CuO, Ag, AgPd(Cu*)
925 O_2	123 + $BaCuO_2$	123(Pd*), 211, CuO, $BaCu(Pd)O_2$, Ag, AgPd(Cu*)
900 O_2	123 + $BaCuO_2$	123(Pd*), 211, CuO, $BaCu(Pd)O_2$, Ag, AgPd(Cu*)
850 O_2	123 + $BaCuO_2$	123(Pd*), 211, CuO, $BaCu(Pd)O_2$, Ag, AgPd(Cu*)

*Indicates values of ≤1 at%, ? indicates some unidentified peaks.

(b) Films quenched from 965°C and 950°C after switching to 100% O_2 (cooling part of Fig. 1) show similar microstructures and phase analyses to those of Fig. 6b. No 123 formation is observed in any quenched film for $T_{quench} \geq 950$°C. However, 123 crystallisation is observed for $T_{quench} \leq 925$°C. The XRD patterns for samples quenched from 925°C or below show a high degree of *c*-axis orientation as well as some $Ba(Cu,Pd)O_2$ phase on the surface, similar to that of Fig. 3b. Reasons can now be suggested as to why crystallisation of 123 is only observed tens of degrees below the peak for the particular processing parameters chosen. The heating and cooling rates used in this study are typical for superconducting thick film processing routes. These rates are relatively fast compared to those used in phase diagram studies, and are chosen to limit reaction between the film and substrate. Because of these fast cooling rates, and a significant nucleation barrier, a large amount of undercooling is required before crystallisation of 123 can occur.

Typical cross-sectional microstructures of the films with $T_{quench} \leq 925$°C are presented in Fig. 7. All three

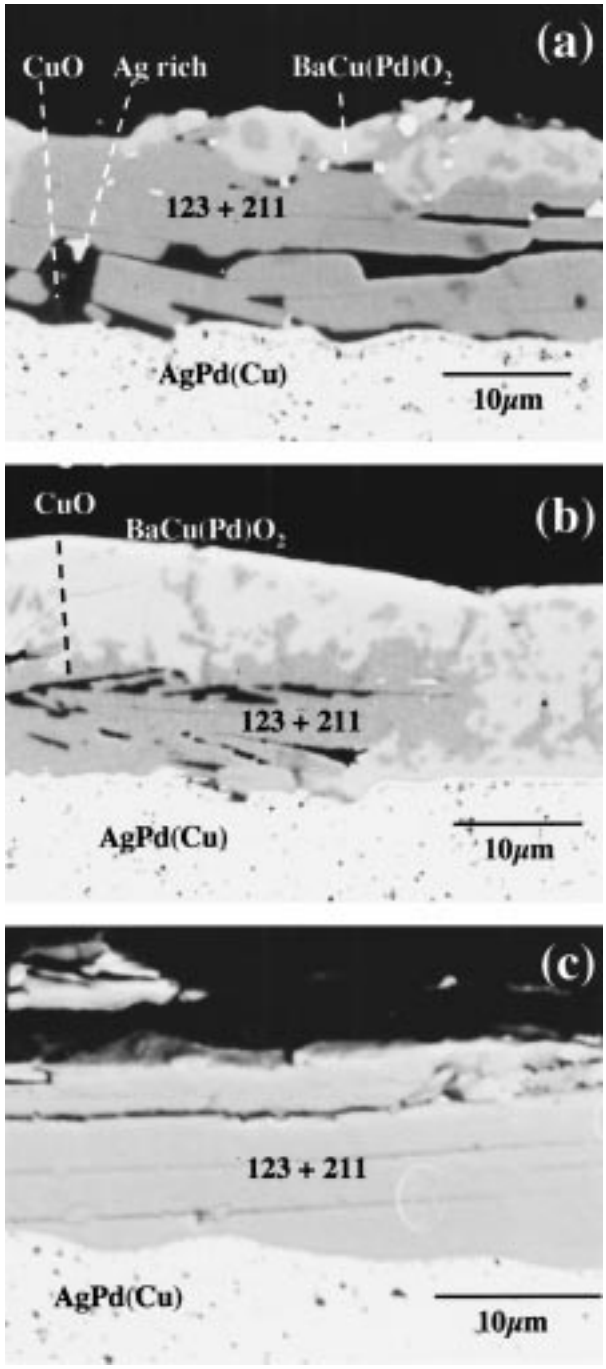

Figure 7 Typical cross-sectional microstructures of superconducting film, $T_{quench} = 900^{\circ}C$.

shown are taken from the same sample ($T_{quench} = 900^{\circ}C$). The morphology is seen to vary along the length of the cross-section. For example, Fig. 7a shows regions of 123 separated by CuO with some $Ba(Cu,Pd)O_2$ on the surface. Fig. 7b is however, dominated by the $Ba(Cu,Pd)O_2$ phase. Fig. 7c shows a well aligned microstructure of textured 123 grains. The J_c behaviour of the films would be enhanced if this type of microstructure were homogeneous over the whole sample cross–section. These types of microstructure are also observed in the slow cooled films for values of $T_{peak} > 970^{\circ}C$.

The presence of Pd in the $Ba(Cu,Pd)O_2$ phase indicates there is a great deal of chemical interaction between the AgPd substrate and film. SEM EDX shows the presence of as much as 8 at% Pd in the $Ba(Cu,Pd)O_2$ phase and ∼1 at% Cu in the Ag substrate near the film/substrate interface. Some of the 123 analyses also reveal evidence for small amounts of Pd substitution (∼1 at% maximum), although it should be stressed these values are at the limit of the accuracy of the EDX measurements. It should also be noted that no Ag was found in any of the analyses of the 123 or $Ba(Cu,Pd)O_2$ phase. As mentioned previously, reaction between YBCO and AgPd has also been seen by other workers. Studies on 123/AgPd composites [12] have suggested that the interaction between 123 and the AgPd reduces the superconducting properties. It is thought that this is due to the replacement of Cu by Pd in the 123 structure. This could explain the low values of J_c observed in the slow cooled samples (Fig. 5). However, recent work on YBCO thick films on AgPd substrates has claimed no observable reaction with the substrate, even for processing temperatures as high as 1030°C [16].

4. Conclusions

YBCO thick films have been prepared on $Ag_{0.85}Pd_{0.15}$ substrates via a screen printing and atmosphere control method. Heating is performed in N_2 to a peak temperature where the atmosphere is switched to O_2, to drive the 123 crystallisation, before cooling. This procedure enables melt processing to take place at lower temperatures than films processed entirely in O_2. Films with enhanced *c*-axis texture and higher values of T_c and J_c are obtained by processing at a peak temperature >970°C. However, the J_c values are still relatively low and this has been attributed to Pd contamination from the substrate. SEM EDX investigations have confirmed chemical interaction between the YBCO film and Pd in the substrate. For example $Ba(Cu,Pd)O_2$ is formed on the surface of the films. Films processed completely in N_2 are found to be non superconducting due to the lack of 123 crystallisation.

Quenching experiments on films heated to a T_{peak} of 980°C have provided information on the phases present at different stages of processing. Initially on heating in N_2, the observations are consistent with the films entering a 211 + 012 + 163 region. EDX and XRD have provided direct evidence for 211 + 012 in this region, whereas indirect evidence for decomposition of the 163 phase or its corresponding liquid is suggested by the presence of $BaCO_3$ in the samples. On switching to O_2 the films pass through the 211 + L region. 211 and Ba-Cu rich phases have been identified from EDX and XRD. For the present cooling rate of 3°C/min, typical for thick film processing, subsequent crystallisation of 123 occurs at a temperature at least 30°C lower than T_{peak}. These films are found to be *c*-axis textured when quenched from ≤925°C, or slow cooled to room temperature.

Acknowledgements

The authors wish to acknowledge The British Council and German Academic Exchange Programme (ARC Project 820) for the provision of funding during this work.

References

1. N. MCN ALFORD, S. J. PENN and T. W. BUTTON, *Supercond. Sci. Technol.* **10** (1997) 169.
2. T. C. SHIELDS, J. B. LANGHORN, S. C. WATCHAM, J. S. ABELL and T. W. BUTTON, *IEEE. Trans. Appl. Supercond.* **7** (1997) 1478.
3. D. J. MOULE, P. D. EVANS, T. C. SHIELDS, S. A. L. FOULDS, J. P. G. PRICE and J. S. ABELL, *ibid.* **7** (1997) 1025.
4. Q. HE, D. K. CHRISTEN, J. D. BUDAI, E. D. SPECHT, D. F. LEE, A. GOYAL, D. P. NORTON, M. PARANTHAMAN, F. A. LIST and D. M. KROEGER, *Physica C* **275** (1997) 155.
5. A. GOYAL, D. P. NORTON, D. M. KROEGER, D. K. CHRISTEN, M. PARANTHAMAN, E. D. SPECHT, J. D. BUDAI, Q. HE, B. SAFFIAN, F. A. LIST, D. F. LEE, E. HATFIELD, P. M. MARTIN, C. E. KLABUNDE, J. MATHIS and C. PARK, *J. Mater. Res.* **12** (1997) 2924.
6. J. WIESMANN, J. HOFFMANN, A. USOSKIN, F. GARCIA-MORENO, K. HEINEMANN and H. C. FREYHARDT, *Inst. Phys. Conf. Ser.* **148** (1995) 503.
7. X. D. WU, S. R. FOLTYN, P. N. ARENDT, W. R. BLUMENTHAL, I. H. CAMPBELL, J. D. COTTON, J. Y. COULTER, W. L. HULTS, M. P. MALEY, H. F. SAFAR and J. L. SMITH, *Appl. Phys. Lett.* **67** (1995) 2397.
8. N. ZAFAR, J. J. WELLS, A. CROSSLEY and J. L. MACMANUS-DRISCOLL, *Inst. Phys. Conf. Series.* **158** (1997) 877.
9. J. L. MACMANUS-DRISCOLL, J. C. BRAVMAN and R. B. BEYERS, *Physica C* **241** (1995) 401.
10. G. KRABBES, W. BIEGER, P. SCHATZLE and U. WIESNER, *Current Topics in Crystal Growth Res.* **2** (1995) 359.
11. K. FISCHER, G. LEITNER, G. FUCHS, M. SCHUBERT, B. SCHLOBACH, A. GLADUN and C. RODIG, *Cryogenics* **33** (1993) 97.
12. M. H. LO and W. C. WEI, *Jap. J. Appl. Phys* **32** (1993) 4509.
13. F. WELLHOFER, T. C. SHIELDS, J. S. ABELL and K. N. R. TAYLOR, *Mat. Res. Soc. Symp. Proc.* **169** (1990) 813.
14. T. W. BUTTON, N. MCN. ALFORD, F. WELLHOFER, T. C. SHIELDS, J. S. ABELL and M. DAY, *IEEE. Trans. Magnetics.* **27** (1991) 1434.
15. F. ABBATTISTA, M. VALLINO, D. MAZZA, M. LUCCO-BORLERA and C. BRISI, *Mat. Chem. Phys.* **20** (1988) 191.
16. X. WEN, D. QU, B. A. TENT, D. SHI, M. TOMSIC and M. WHITE, *Proc. IEEE Appl. Supercond.* **9** (1999) 1506.

Received 6 October 1999
and accepted 17 May 2000